ACS Photonics

Article

pubs.acs.org/journal/apchd5

Gap-Plasmon Enhanced Gold Nanoparticle Photoluminescence

Chatdanai Lumdee,[†] Binfeng Yun,[‡] and Pieter G. Kik*[,†,§]

[†]CREOL, The College of Optics and Photonics, and [§]Physics Department, University of Central Florida, 4000 Central Florida Boulevard, Orlando, Florida 32816, United States

[‡]Advanced Photonics Center, School of Electronic Science and Engineering, Southeast University, Nanjing 210096, China

Supporting Information

ABSTRACT: Gap-plasmon-enhanced gold nanoparticle photoluminescence is studied experimentally at the single-particle level. The photoluminescence spectra of gold nanoparticles on an Al_2O_3-coated gold film under both 532 and 633 nm excitation show a clear peak near the measured gap-plasmon resonance wavelength. Comparing the collected emission spectrum with that from a gold reference film under 633 nm excitation, a peak photoluminescence enhancement factor of 28 000 is observed. The spectral shape and absolute magnitude of the enhancement factors for both excitation wavelengths are reproduced using numerical calculations without the use of any free parameters. The photoluminescence enhancement is explained in terms of a gap-mode-enhanced e−h pair generation rate and a wavelength-dependent enhancement of the emission efficiency.

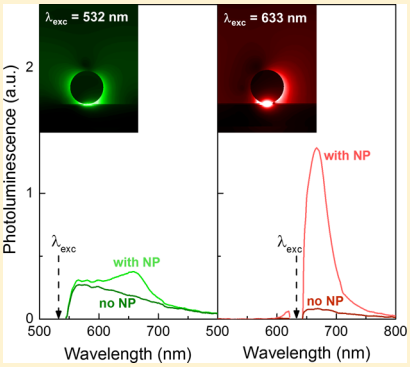

KEYWORDS: *gap plasmon, gap mode, plasmon resonance, gold nanoparticle, gold photoluminescence, photoluminescence enhancement*

The first observation of gold photoluminescence (PL) was reported in 1969 by Mooradian, who observed a broad unpolarized emission spectrum with an emission peak at ∼500 nm. These findings were attributed to radiative recombination of holes in the d-band with electrons in the sp-band[1] with an estimated emission quantum efficiency on the order of 10^{-10}. In 1986 Boyd et al. developed a detailed model describing the photoluminescence from roughened metal films in terms of band structure and field enhancement factors. By describing the rough surface as a random collection of grounded nanoscale hemispheres and considering the field enhancement at the excitation and emission wavelengths, good agreement between measured and experimental photoluminescence data was obtained.[2] Since those early observations advances in nanofabrication have enabled the systematic investigation of photoluminescence from large collections of gold nanostructures. Such ensemble measurements revealed an unusually strong PL signal, which unlike that observed in bulk gold shows emission peaks that correlate with plasmon-related peaks in the extinction spectra, suggesting that surface plasmons are involved in the emission enhancement.[3−7] More recently, advances in microscopy and spectroscopy techniques have enabled the investigation of the PL response of individual gold nanostructures. These single-particle studies demonstrated a close correlation between the PL spectra and their scattering spectra and confirmed the increase in PL quantum yield compared to bulk gold.[8−12] Moreover, it was observed that the enhanced PL from anisotropic gold nanostructures results in emission with a polarization angle aligned with the polarization direction of a spectrally matched plasmon resonance, even when the structure is excited at frequencies far from the resonance.[12−14] Most studies describe the enhancement in terms of a plasmon-enhanced e−h pair generation rate and a plasmon-enhanced radiative recombination efficiency, both associated with the enhanced local electric fields that occur near the plasmon resonance frequency. In addition it has recently been proposed that excitation of high-angular-momentum plasmons can become a major nonradiative e−h recombination channel for holes located near the metal surface.[15] Despite the general agreement on the main contributing factors to the fluorescence enhancement, few studies quantitatively analyze these effects at the single-particle level.[4−7,11−14]

A plasmonic system that has recently received a significant amount of attention is the film-coupled nanoparticle system. Metal particles deposited on metallic or highly polarizable substrates or films exhibit resonances that are strongly localized near the gap between the particle and the substrate. The field enhancement provided by such gap plasmons can significantly exceed that of individual nanosphere resonators, and it has been used in plasmon-mediated optical sensing applications including the detection of local chemical reactions[16] and surface-enhanced Raman scattering of molecules.[17−20] This structure is also of interest due to its ability to generate energetic electrons and holes in the important junction region of a nanoparticle with a dielectric-coated substrate, which may have applications in plasmon-enhanced (internal) photoemission and plasmon-mediated photocatalysis.[21−24] In addition, film-coupled nanoparticles offer several advantages over

Received: August 14, 2014
Published: October 8, 2014

other coupled plasmonic resonators that support gap plasmons. These include their ease of fabrication, their highly reproducible optical response, their structural stability, and their wideband spectral tunability through variation of the particle−substrate separation.[25−27] These factors make film-coupled nanospheres a promising platform for the quantitative analysis of plasmon-enhanced gold photoluminescence and related electronic effects. The present study uses a combination of single-particle scattering spectroscopy and single-particle multiwavelength excited photoluminescence spectroscopy to determine the magnitude and physical origin of the gold PL enhancement by gap plasmons. A numerical approach is presented that achieves quantitative agreement between the observed and modeled PL enhancement spectra. We show a maximum measured PL enhancement factor as high as 28 000 at the gap-mode resonance wavelength, relative to the PL signal obtained from a planar gold film with an area equal to the physical cross-section of the nanoparticle.

RESULTS AND DISCUSSION

To generate a structure supporting gap plasmons, 80 nm diameter gold nanoparticles were deposited from a colloidal solution onto an aluminum oxide (Al_2O_3)-coated gold film with a measured Al_2O_3 thickness of 3.4 nm. This results in the formation of a well-defined nanostructure with a plasmon resonance wavelength in the visible range. Details of the experimental and numerical procedures are provided in the Methods section. Figure 1a shows a dark-field microscopy image of the gold nanoparticles sparsely distributed on the Al_2O_3-coated gold film. The film-coupled nanoparticles predominantly scatter red light and appear ring-shaped, characteristic of a vertically polarized gap-mode plasmon resonance.[25,28,29] Note that all gold nanoparticles have similar scattering color and intensity, indicating that all particles support similar plasmon resonances. Figure 1b presents the peak-normalized measured scattering spectrum I_{scat} (solid line) of the nanoparticle highlighted by the white dashed square in Figure 1a. The scattering spectrum has a strong resonance peak at ∼650 nm with a full width at half-maximum (fwhm) of ∼68 nm and a small shoulder at a wavelength of ∼550 nm. Spectral measurements on several other particles reveal typical variations in peak scattering wavelength on the order of ±10 nm. For additional representative spectra see the Supporting Information. Numerical simulations of the scattering spectrum were carried out to identify the modes responsible for the features in the experimental scattering spectrum. Figure 1c shows the simulated scattering spectrum of an 80 nm diameter spherical Au nanoparticle on a gold film coated with a 2.8 nm Al_2O_3 film, close to the experimentally determined Al_2O_3 thickness. The simulations reproduce the experimentally observed scattering peak position of 652 nm, as well as the presence of a secondary peak at shorter wavelength. Figure 1d and e show the simulated distribution of the electric field magnitude relative to the incoming field at 550 nm and at 652 nm, respectively. Note that in both cases the field enhancement factor near the gap exceeds the plotting range. The main resonance peak at 652 nm is seen to correspond to a highly confined plasmon mode with most of the field concentrated near the gap between the particle and the gold film (gap plasmon).[29] At this frequency the peak field amplitude 1 nm inside the gold particle exceeds the incident field strength by a factor 17 under TM illumination. Unlike the more common situation of spherical and ellipsoidal nanoparticles suspended in solution, the field enhancement is highly

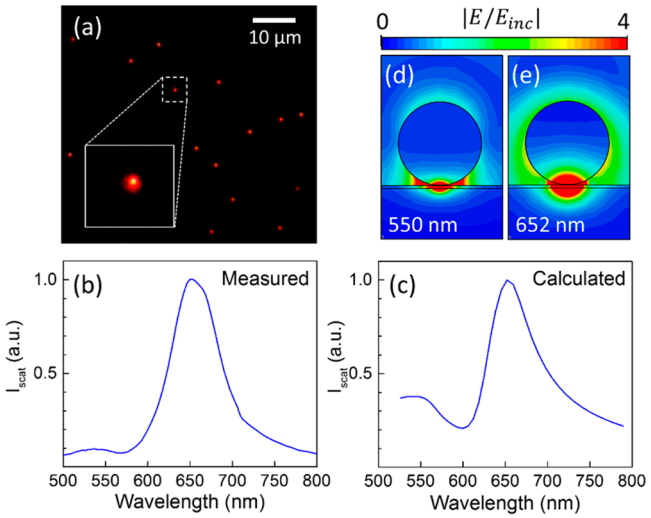

Figure 1. (a) Dark-field microscopy image of 80 nm diameter gold nanoparticles on an Al_2O_3-coated gold film. (b and c) Measured and simulated scattering spectra of the gold nanoparticle highlighted in (a). (d and e) The simulated distribution of the electric field magnitude under illumination at respectively 550 and 652 nm TM at an angle of incidence of 77°, corresponding to the experimental dark-field illumination angle.

inhomogeneous, complicating the analysis of related optical effects. The electric field distribution under 550 nm excitation shows the presence of a higher order resonance with lower overall field enhancement than the main resonance. This mode appears relatively prominent in the simulated scattering spectrum in Figure 1c compared to the experimental results. This difference may be due to the fact that the simulations do not take into account the nonlocal nature of the metal dielectric function, which is known to suppress modes exhibiting significant field variation over a typical distance v_f/f with v_f the Fermi velocity and f the plasmon resonance frequency through a process known as Landau damping.[30] In gold at 550 nm this distance is 2.5 nm, which is indeed comparable to the spatial field variation near the gap of the electric field distribution at 550 nm in Figure 1d.

Photoluminescence measurements of individual gold nanoparticles were carried out using continuous wave excitation at either 532 or 633 nm. The experimental setup is shown schematically in Figure 2. A 100 μW laser beam (532 or 633 nm) is sent into the microscope via a laser port and directed off-center to the microscope objective, leading to p-polarized illumination at the sample surface at a measured angle of incidence of ∼35°. The fwhm of the laser spot at both wavelengths was determined to be ∼2.8 ± 0.2 μm using the nanoparticle-mediated beam sampling method described in ref 26. This excitation geometry provides the surface-normal electric field component needed to excite the gap mode on the Au nanoparticles. This is illustrated by the simulation results in Figure 2b and c, showing a snapshot of the z-component of the electric field under p-polarized excitation respectively at 532 and 633 nm at an angle of 35°, scaled to the same field value. These excitation wavelengths are close to the gap-mode resonance wavelengths, and indeed in both cases the excited field distribution is seen to be strongly confined in the gap. Note that the mode excited at 532 nm exhibits a higher spatial frequency along the particle perimeter and lower internal field strength compared to the mode excited at 633 nm.

dx.doi.org/10.1021/ph500304v | ACS Photonics 2014, 1, 1224−1230

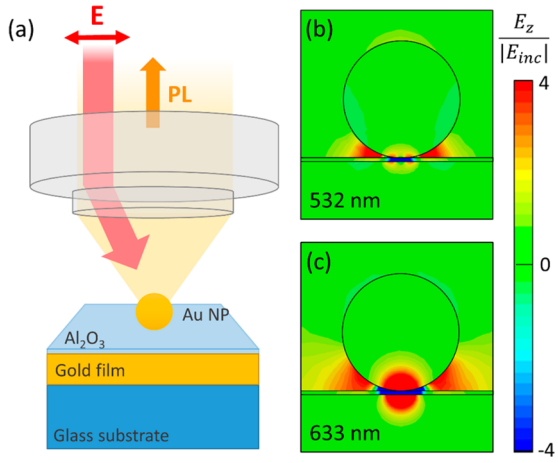

Figure 2. (a) Experimental configuration for single-particle photoluminescence spectroscopy. (b and c) Snapshots of the simulated electric field distributions respectively under 532 and 633 nm excitation at an angle of incidence of 35°, corresponding to the experimental laser excitation angle.

Figure 3a shows gold photoluminescence spectra collected under 532 nm excitation, obtained from the sample shown in Figure 1a. Since the laser spot size is much smaller than the typical interparticle separation, it is possible to selectively excite a region of the Au film that does not contain nanoparticles. The dark green line shows such a reference measurement collected from a region near the nanoparticle, resulting in a broad featureless emission spectrum with a short-wavelength onset governed by the long-pass filter used to suppress Rayleigh scattering. This emission is commonly attributed to the excitation of d-band electrons to the sp-band followed by radiative carrier recombination.[2,31] On the basis of the absorbed laser power, the collection efficiency, and the integrated photon count, the quantum efficiency of the detected photoluminescence is estimated to be 3×10^{-10}. This matches typical numbers reported in the literature, providing further evidence that the collected signal originates from the gold film.[1] The bright green line in Figure 3a shows the PL signal collected when the nanoparticle highlighted in Figure 1a is moved into the center of the excitation spot. In this case a similar broad luminescence background is present; however additional signal appears near the nanoparticle gap mode resonance wavelength, resulting approximately in a doubling of the PL signal at 660 nm. Remarkably, this signal doubling is achieved using a particle that has a physical cross-section 3 orders of magnitude smaller than the laser spot area; see the left sketch in Figure 3a. Figure 3b shows the corresponding data under 633 nm excitation. In this case the signal from an area not containing a nanoparticle (dark red line) is again broad and featureless, but a factor 2.4 weaker than when excited with green light. This reduction in signal is attributed to the fact that at this lower excitation energy fewer interband transitions are available, as evident from the Au band structure and the Au dielectric function, leading to a reduced e–h pair generation rate. Note that the spectrum shows a narrowband dip near the laser line. This is caused by the response of the notch filter that was used to suppress Rayleigh scattering of the excitation laser. The PL signal from the area containing the nanoparticle (bright red line) is remarkably strong under 633 nm excitation, exceeding the corresponding background signal by a factor ~16 at the main gap-plasmon resonance wavelength. The nanoparticle (NP)-enhanced PL emission appears to have a different spectral shape under different excitation conditions, which is largely due to the different relative contribution of NP-mediated PL and the Au film PL background in these two cases; see the Supporting Information. No experimental evidence was found for photoluminescence excited via propagating surface plasmon polaritons on the gold surface.

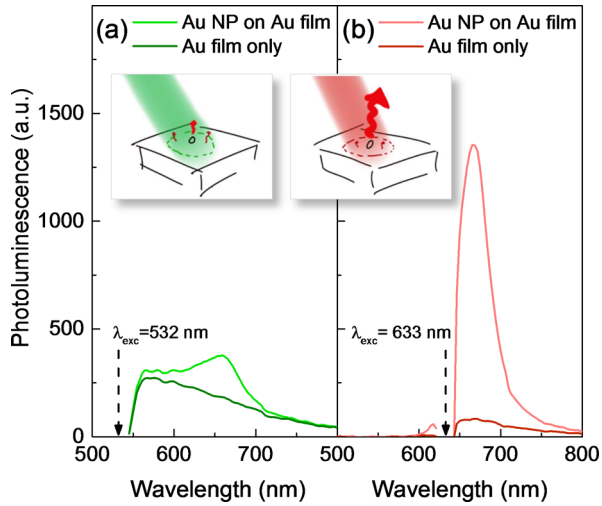

Figure 3. Photoluminescence spectra collected under 532 nm excitation (a) and 633 nm excitation (b) from areas containing a gold nanoparticle (bright green and bright red lines) and no gold nanoparticle (dark green and dark red lines). The insets schematically show that a gold nanoparticle adds PL signal at the particle resonance wavelength (red arrows) to the weak background PL.

To investigate the nanoparticle-mediated PL enhancement quantitatively, we define a photoluminescence enhancement factor g_{PL} as

$$g_{PL}(\lambda_{exc}, \lambda_{em}) = \frac{I_{NP} - I_{film}}{I_{film}} \frac{A_{eff}}{\sigma_{NP}} \quad (1)$$

where I_{NP} is the PL signal collected when illuminating an area containing a particle, I_{film} is the signal collected from a substrate area away from the particle, A_{eff} is the effective laser spot area defined as $A_{eff} = \pi R_{1/e}^2$ with $R_{1/e}$ the spot radius at $1/e$ of the peak irradiance, and σ_{NP} is the physical cross-section of the NP. With this definition, the enhancement factor represents the PL signal added by the presence of the particle, relative to the PL signal from a substrate area with a size equal to the physical cross-section of the particle excited at the same irradiance. This enhancement factor is independent of the laser spot size, does not depend on the intrinsic wavelength-dependent e–h generation efficiency, and does not depend on the intrinsic wavelength-dependent emission efficiency. Figure 4a shows the experimentally obtained PL enhancement spectra g_{PL} for the gold nanoparticle highlighted in Figure 1a excited with 532 and 633 nm laser beams (green and red solid lines, respectively), based on the curves in Figure 3 and the measured laser spot sizes. For comparison the peak-normalized scattering spectrum of the particle has been included (black dashed line, right axis). Several features should be noted. First, the maximum PL enhancement occurs close to the main plasmon resonance wavelength of the nanoparticle. Second, the shape of the enhancement spectrum appears identical for the two excitation wavelengths. Third, the overall enhancement factors achieved

dx.doi.org/10.1021/ph500304v | ACS Photonics 2014, 1, 1224–1230

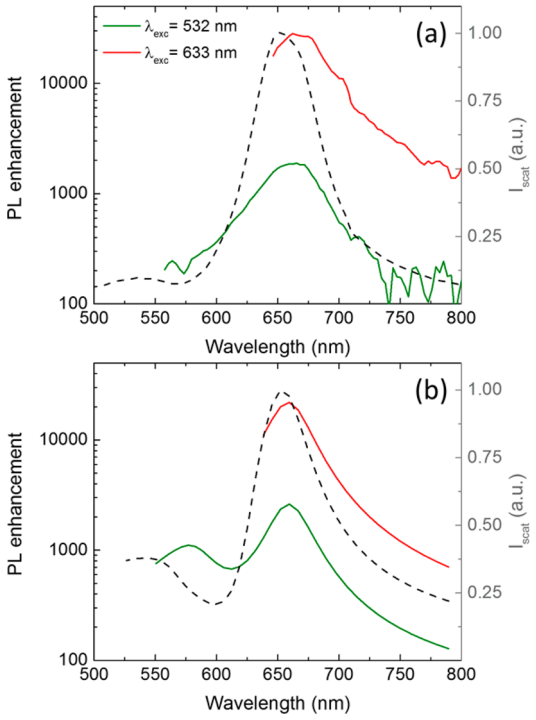

Figure 4. Measured (a) and calculated (b) photoluminescence enhancement spectra g_{PL} for a gold nanoparticle excited with 532 nm (green solid lines) and 633 nm (red solid lines) laser lines. The black dashed lines show the measured and calculated peak-normalized scattering spectra of the particle.

under 633 nm excitation are approximately an order of magnitude larger than under 532 nm excitation. These observations reproduce quantitatively when considering different particles on the same sample; see the Supporting Information. The largest enhancement is achieved near the gap-mode resonance under excitation near the resonance frequency, showing a peak enhancement factor of 28 000.

To understand the observations in Figure 4, we quantitatively model the photoluminescence enhancement factor by evaluating the nanoparticle-induced changes in e−h generation rate and emission efficiency based on simulated electric field distributions. The electron−hole pair generation rate in a volume element dV inside gold is proportional to $\varepsilon''_{IB}|\vec{E}_{TM}(\vec{r},\omega)|^2$ where ω is the angular frequency of the excitation source, $\varepsilon''_{IB}(\omega)$ is the part of the imaginary dielectric function related to interband transitions at the excitation frequency, and $\vec{E}_{TM}(\vec{r},\omega)$ is the simulated field distribution under TM excitation at the experimental angle of incidence (see Figure 2b and c for the corresponding field cuts). To determine the enhancement of the emission efficiency, we make several assumptions. First, we assume that radiative e−h recombination in the gold film is highly inefficient and remains highly inefficient in the presence of the nanoparticle. In this case any changes in emission rate are accompanied by an improvement of the emission efficiency by the same factor. Second, we assume that the radiative emission rate into a given narrow angular range is proportional to the simulated local electric field intensity under plane wave excitation at an angle in that range. Third, we assume that the collected PL spectrum is dominated by signal emitted at the a typical collection angle of 35°. Since radiative recombination may lead to s- or p-polarized emission, we take into account simulated fields $E_{TM}(\omega_{em})$ and $E_{TE}(\omega_{em})$ for TM and TE polarization, where ω_{em} represents the angular frequency of the emitted light. Finally, we assume that carrier movement during the e−h recombination time is negligible relative to the spatial extent of the excitation field, allowing us to model excitation and emission enhancement based on simulated electric fields at a single position $\vec{r}$. On the basis of these assumptions, the emission rate R_{PL} from a volume element near position $\vec{r}$ excited at ω_{exc} is proportional to

$$R_{PL}(\omega_{exc}, \omega_{em}) \propto \varepsilon''_{IB}(\omega_{exc})|\vec{E}(\omega_{exc})|^2 \times \gamma(\omega_{exc}, \omega_{em}) \left[\left|\frac{E_{TE}(\omega_{em})}{E_0(\omega_{em})}\right|^2 + \left|\frac{E_{TM}(\omega_{em})}{E_0(\omega_{em})}\right|^2\right] \quad (2)$$

where γ is a function describing the bulk gold photoluminescence spectrum under excitation at ω_{exc}. Position arguments have been omitted for brevity. The total gold photoluminescence in the presence of a gold nanoparticle (I_{NP}) can now be calculated in relative units based on the simulated field distributions by integration of eq 2 throughout the particle volume and the Au film, while I_{film} can be determined similarly from simulated field distributions in the absence of a nanoparticle. The resulting spectra allow us to predict the absolute PL enhancement factor g_{PL} quantitatively using eq 1 without the use of any free parameters for a given simulation geometry.

Figure 4b presents the resulting simulated PL enhancement spectrum g_{PL} for excitation at 532 nm (green solid line) and 633 nm (red solid line) of the structure shown in Figure 2. The peak-normalized calculated scattering spectrum is included for comparison (black dashed line). The simulated results show remarkable agreement with the experimentally determined enhancement spectra. First, the maximum simulated enhancement factor under excitation at 633 nm is 22 000, only 22% lower than the experimentally determined value, despite the sensitivity of the result on the laser spot size and particle alignment in the laser spot. It bears repeating that this correspondence is obtained without the use of any free parameters. Second, the simulated PL enhancement under 532 nm excitation is a factor of 8 lower than under 633 nm excitation, compared to a factor of 15 in the experiment. Third, the simulated enhancement spectra have a nearly identical shape for different excitation wavelengths, as is also observed experimentally. Finally, the maximum simulated enhancement appears at slightly longer wavelengths than the scattering peak wavelength. Numerical simulations indicate that this small shift is a result of the difference in excitation angle for the scattering spectroscopy and PL measurements.

Given the good correspondence between the experimental and numerical results, we are able to assign the physical origin of the various experimental observations. Figure 5 illustrates the contributing factors to the PL enhancement under excitation at 532 nm. Figure 5b shows the Au band structure around the X point adapted from ref 32 with the energy of the top of the d-band set to 0 eV and energies below the Fermi level marked by the shaded region. Excitation of a gold film with 532 nm light can excite d-band electrons into empty sp-band states (green vertical arrow), followed by electron and hole relaxation and eventual electron−hole recombination. From the experimental scattering spectrum shown in Figure 5a it is clear that this green light (energy marked by the green dashed line) interacts with the higher order plasmon mode, resulting in slightly enhanced e−h generation in the Au nanoparticle gap region, in addition

dx.doi.org/10.1021/ph500304v | ACS Photonics 2014, 1, 1224−1230

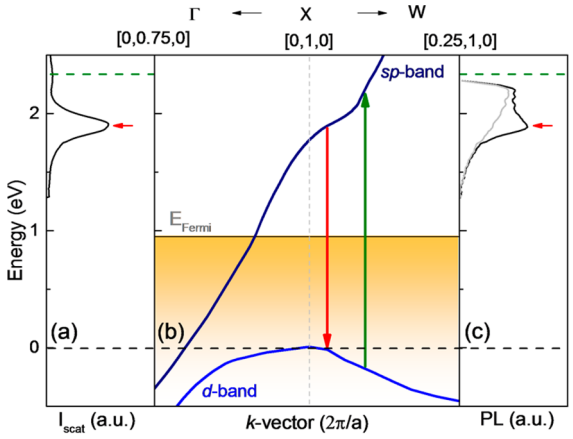

Figure 5. (a and c) Measured scattering and photoluminescence spectra of a film-coupled gold nanoparticle. The dashed green lines mark the photon energy corresponding to 532 nm excitation. The horizontal red arrows indicate the gap-plasmon resonance energy. (b) Au band structure around the X point near the Fermi level, adapted from ref 32. The vertical green and red arrows show e–h excitation at 532 nm followed by plasmon-enhanced recombination at an e–h energy separation that matches the gap-plasmon resonance energy.

to the e–h pairs generated in the gold film. This excitation enhancement slightly increases the total PL intensity in this case and does not affect the spectral shape of the emission. During relaxation of the generated energetic carriers, a small probability of radiative recombination exists. Since the extra e–h pairs are predominantly excited near the gap (see Figure 2b), they experience a strongly enhanced local optical density of states associated with the gap-plasmon mode, leading to an enhancement of the emission rate. Consequently, the observation of large enhancement factors requires spatial overlap of the plasmon-enhanced e–h generation profile with the field distribution of the plasmon mode that is responsible for the emission enhancement. When the energy difference between the electron and the hole during relaxation matches that of the gap-plasmon resonance (marked by the red horizontal arrows in Figure 5a and c), the recombination rate is maximally enhanced, coupling energy into the gap mode, which subsequently radiates into the far field. Figure 5c shows the corresponding experimental PL spectra under 532 nm excitation of a flat gold film (gray line) and of a gold nanoparticle on the film (black line). For excitation at 633 nm, the mechanism is similar, but the excitation photon energy is closer to the gap-mode resonance energy, resulting in a stronger enhancement of the e–h generation rate. In addition, the excitation field distribution is almost exactly matched to that of the gap mode, maximizing the fraction of e–h pairs that can interact with the gap mode. Together these effects explain the larger overall PL enhancement factors observed under 633 nm excitation compared to those observed under 532 nm excitation. Note that under 532 nm excitation, e–h pair generation and therefore radiative recombination can occur near both the X point and the L point in the Au band structure, as discussed in detail in ref 8. It has been suggested that the radiative recombination efficiencies from these two types of e–h pairs could be different, which in principle could affect our analysis. The good correspondence between our measured and simulated enhancement factors suggests that such differences do not have a major effect on the magnitude of the enhancement factor in this system. This may be due to the fact that the radiative recombination efficiencies for either class of e–h pairs are much smaller than unity, and consequently for both classes of e–h pairs an increase in the radiation rate will lead to a linearly proportional increase in the emission efficiency.

While the numerical simulations and the physical model description are able to quantitatively describe the key aspects of the experimentally observed enhancement spectra, differences are observed. Most notably the simulated PL enhancement spectra exhibit a pronounced shoulder near 580 nm that is not observed in the experimental data. This shoulder is caused by the higher order resonance observed in the simulations; see Figure 2b. As argued before, this mode is expected to be relatively highly damped due to nonlocal effects that are not accounted for in the simulations, resulting in an overestimation of the field enhancement and therefore of the e–h excitation enhancement. A final point worth noting is that the gap-mode-enhanced photoluminescence does not originate exclusively from the Au nanoparticle. On the basis of the simulations, we find that the extra PL contributed by the gap-mode plasmon resonance (λ = 660 nm) originates largely from the region inside the Au nanoparticle closest to the substrate (~70%), while the region of the gold film directly underneath the nanoparticle contributes ~30% of the added PL signal.

CONCLUSION

In conclusion, we have measured plasmonic gap-mode-enhanced photoluminescence of a gold nanoparticle on an Al_2O_3-coated gold film. A PL enhancement factor was defined making use of the PL signal collected from a gold film reference, and based on this definition a maximum PL enhancement factor of 28 000 under 633 nm excitation was obtained. Numerical simulations were shown to reproduce the excitation wavelength dependence, the spectral shape of the enhancement, and the absolute enhancement factors without the use of any free parameters. The enhancement could be explained entirely in terms of a plasmon-enhanced e–h pair generation, combined with an increase in the emission rate associated with the electric field enhancement near the particle–substrate contact point.

METHODS

An Al_2O_3-coated gold film was prepared by thermal evaporation using a multipocket Edwards FL 400 thermal evaporator. A 2 nm thick chromium wetting layer was deposited onto a glass coverslip (Thermo Scientific), immediately followed by the thermal evaporation of a 50 nm gold film. A few-nanometer-thick aluminum layer was deposited on the gold layer without breaking vacuum. The aluminum film completely oxidizes into an Al_2O_3 layer after exposure to air. The Al_2O_3 thickness was measured using variable-angle spectroscopic ellipsometry and was found to be 3.4 nm. Gold nanoparticles were drop-coated on the substrate and left to dry in air from an ethanol-diluted monodispersed gold nanoparticle colloidal solution (BBInternational) with a particle diameter of 80.7 nm (size variation σ < 3.9%).

Optical microscopy and spectroscopy were performed on an Olympus IX-71 inverted microscope equipped with standard dark-field optics using a 50× dark-field objective (Olympus UMPlanFl 50× BD, collection NA = 0.75, 77° illumination angle). Dark-field images and single-particle spectra were recorded using a Canon EOS 450D digital camera and an

dx.doi.org/10.1021/ph500304v | ACS Photonics 2014, 1, 1224–1230

imaging spectrometer (Horiba iHR320 spectrometer equipped with an Andor DU401-BR-DD CCD camera), respectively. The large interparticle separation allows for the spatial selection of individual nanoparticles for spectroscopy by limiting the spectrometer entrance slit width and using vertical binning of the recorded CCD data (collection area ~6 × 4 μm^2). All spectra were collected with a 10 seconds exposure time and corrected for the detector dark current. The raw spectra were averaged over 18 pixels to match the optical spectral resolution of 10 nm. The scattering spectrum of gold nanoparticles was obtained by collecting the scattered signal from the particle (I_{NP}), subtracting the scattered signal from a nearby area without a nanoparticle (I_{ref}), and dividing by the latter, corresponding to the formula $I_{scat} = (I_{NP} - I_{ref})/I_{ref}$.

For single-particle PL measurements each nanoparticle was aligned to the center of the laser spot using a three-axis piezocontrolled sample stage. The reflected laser beam was blocked using a beam stop, and any remaining Rayleigh scattered laser light was suppressed using a 550 nm long-pass filter in the case of 532 nm excitation and a notch filter in the case of 633 nm excitation. Photoluminescence spectra were recorded under 100 μW continuous wave irradiation with the same collection system as used in the scattering spectroscopy but using a 60 seconds integration time and ~6 × 10 μm^2 collection area. All spectra were corrected for the detector dark current and the grating and detector spectral response functions.

Frequency domain full-field electromagnetic simulations were carried out using CST Microwave Studio[33] assuming a unit cell boundary condition with a lateral cell size of 240 nm × 240 nm. Plane waves with TE and TM polarization were used as the excitation sources. Simulated electric field distributions at an angle of incidence of 77° and 35° were used to calculate the gold particle scattering spectrum and PL enhancement spectrum, respectively. Literature data were used for the dielectric functions of gold and Al_2O_3.[34,35] The scattering spectrum of a gold nanoparticle was calculated using the method described in ref 26. Briefly, the calculated electric fields in the particle and the gold film were first used to calculate the total electric dipole of the structure (μ). The scattering spectrum is assumed to be proportional to the dipole radiation power: $I_{scat} \propto \omega^4|\mu|^2$.[36]

■ ASSOCIATED CONTENT

Supporting Information

Scattering and photoluminescence enhancement spectra from additional single gold nanoparticles and a short discussion on the spectral shape of nanoparticle photoluminescence spectra under two different excitation wavelengths are provided in the Supporting Information. This material is available free of charge via the Internet at http://pubs.acs.org.

■ AUTHOR INFORMATION

Corresponding Author

*E-mail: kik@creol.ucf.edu.

Author Contributions

The manuscript was written through contributions of all authors. All authors have given approval to the final version of the manuscript.

Notes

The authors declare no competing financial interest.

■ ACKNOWLEDGMENTS

Part of this work was funded by the China State Scholarship Foundation (No. 2010832300).

■ REFERENCES

(1) Mooradian, A. Photoluminescence of Metals. *Phys. Rev. Lett.* **1969**, *22*, 185−187.

(2) Boyd, G. T.; Yu, Z. H.; Shen, Y. R. Photoinduced Luminescence from the Noble-Metals and Its Enhancement on Roughened Surfaces. *Phys. Rev. B* **1986**, *33*, 7923−7936.

(3) Wilcoxon, J. P.; Martin, J. E.; Parsapour, F.; Wiedenman, B.; Kelley, D. F. Photoluminescence from Nanosize Gold Clusters. *J. Chem. Phys.* **1998**, *108*, 9137−9143.

(4) Mohamed, M. B.; Volkov, V.; Link, S.; El-Sayed, M. A. The 'Lightning' Gold Nanorods: Fluorescence Enhancement of over a Million Compared to the Gold Metal. *Chem. Phys. Lett.* **2000**, *317*, 517−523.

(5) Varnavski, O. P.; Mohamed, M. B.; El-Sayed, M. A.; Goodson, T. Relative Enhancement of Ultrafast Emission in Gold Nanorods. *J. Phys. Chem. B* **2003**, *107*, 3101−3104.

(6) Dulkeith, E.; Niedereichholz, T.; Klar, T. A.; Feldmann, J.; von Plessen, G.; Gittins, D. I.; Mayya, K. S.; Caruso, F. Plasmon Emission in Photoexcited Gold Nanoparticles. *Phys. Rev. B* **2004**, *70*, 205424.

(7) Varnavski, O. P.; Goodson, T.; Mohamed, M. B.; El-Sayed, M. A. Femtosecond Excitation Dynamics in Gold Nanospheres and Nanorods. *Phys. Rev. B* **2005**, *72*, 235405.

(8) Beversluis, M. R.; Bouhelier, A.; Novotny, L. Continuum Generation from Single Gold Nanostructures through near-Field Mediated Intraband Transitions. *Phys. Rev. B* **2003**, *68*, 115433.

(9) Bouhelier, A.; Bachelot, R.; Lerondel, G.; Kostcheev, S.; Royer, P.; Wiederrecht, G. P. Surface Plasmon Characteristics of Tunable Photoluminescence in Single Gold Nanorods. *Phys. Rev. Lett.* **2005**, *95*, 267405.

(10) Steiner, M.; Debus, C.; Failla, A. V.; Meixner, A. J. Plasmon-Enhanced Emission in Gold Nanoparticle Aggregates. *J. Phys. Chem. C* **2008**, *112*, 3103−3108.

(11) Fang, Y.; Chang, W. S.; Willingham, B.; Swanglap, P.; Dominguez-Medina, S.; Link, S. Plasmon Emission Quantum Yield of Single Gold Nanorods as a Function of Aspect Ratio. *ACS Nano* **2012**, *6*, 7177−7184.

(12) Hu, H. L.; Duan, H. G.; Yang, J. K. W.; Shen, Z. X. Plasmon-Modulated Photoluminescence of Individual Gold Nanostructures. *ACS Nano* **2012**, *6*, 10147−10155.

(13) Tcherniak, A.; Dominguez-Medina, S.; Chang, W. S.; Swanglap, P.; Slaughter, L. S.; Landes, C. F.; Link, S. One-Photon Plasmon Luminescence and Its Application to Correlation Spectroscopy as a Probe for Rotational and Translational Dynamics of Gold Nanorods. *J. Phys. Chem. C* **2011**, *115*, 15938−15949.

(14) Yorulmaz, M.; Khatua, S.; Zijlstra, P.; Gaiduk, A.; Orrit, M. Luminescence Quantum Yield of Single Gold Nanorods. *Nano Lett.* **2012**, *12*, 4385−4391.

(15) Shahbazyan, T. V. Theory of Plasmon-Enhanced Metal Photoluminescence. *Nano Lett.* **2013**, *13*, 194−198.

(16) Tittl, A.; Yin, X.; Giessen, H.; Tian, X. D.; Tian, Z. Q.; Kremers, C.; Chigrin, D. N.; Liu, N. Plasmonic Smart Dust for Probing Local Chemical Reactions. *Nano Lett.* **2013**, *13*, 1816−1821.

(17) Hill, R. T.; Mock, J. J.; Urzhumov, Y.; Sebba, D. S.; Oldenburg, S. J.; Chen, S. Y.; Lazarides, A. A.; Chilkoti, A.; Smith, D. R. Leveraging Nanoscale Plasmonic Modes to Achieve Reproducible Enhancement of Light. *Nano Lett.* **2010**, *10*, 4150−4154.

(18) Chen, S. Y.; Mock, J. J.; Hill, R. T.; Chilkoti, A.; Smith, D. R.; Lazarides, A. A. Gold Nanoparticles on Polarizable Surfaces as Raman Scattering Antennas. *ACS Nano* **2010**, *4*, 6535−6546.

(19) Mubeen, S.; Zhang, S. P.; Kim, N.; Lee, S.; Kramer, S.; Xu, H. X.; Moskovits, M. Plasmonic Properties of Gold Nanoparticles Separated from a Gold Mirror by an Ultrathin Oxide. *Nano Lett.* **2012**, *12*, 2088−2094.

(20) Li, L.; Hutter, T.; Steiner, U.; Mahajan, S. Single Molecule Sers and Detection of Biomolecules with a Single Gold Nanoparticle on a Mirror Junction. *Analyst* **2013**, *138*, 4574−4578.
(21) Knight, M. W.; Sobhani, H.; Nordlander, P.; Halas, N. J. Photodetection with Active Optical Antennas. *Science* **2011**, *332*, 702−704.
(22) Liu, Z. W.; Hou, W. B.; Pavaskar, P.; Aykol, M.; Cronin, S. B. Plasmon Resonant Enhancement of Photocatalytic Water Splitting under Visible Illumination. *Nano Lett.* **2011**, *11*, 1111−1116.
(23) Thomann, I.; Pinaud, B. A.; Chen, Z. B.; Clemens, B. M.; Jaramillo, T. F.; Brongersma, M. L. Plasmon Enhanced Solar-to-Fuel Energy Conversion. *Nano Lett.* **2011**, *11*, 3440−3446.
(24) Christopher, P.; Xin, H. L.; Marimuthu, A.; Linic, S. Singular Characteristics and Unique Chemical Bond Activation Mechanisms of Photocatalytic Reactions on Plasmonic Nanostructures. *Nat. Mater.* **2012**, *11*, 1044−1050.
(25) Lumdee, C.; Toroghi, S.; Kik, P. G. Post-Fabrication Voltage Controlled Resonance Tuning of Nanoscale Plasmonic Antennas. *ACS Nano* **2012**, *6*, 6301−6307.
(26) Lumdee, C.; Yun, B.; Kik, P. G. Wide-Band Spectral Control of Au Nanoparticle Plasmon Resonances on a Thermally and Chemically Robust Sensing Platform. *J. Phys. Chem. C* **2013**, *117*, 19127−19133.
(27) Ciraci, C.; Chen, X. S.; Mock, J. J.; McGuire, F.; Liu, X. J.; Oh, S. H.; Smith, D. R. Film-Coupled Nanoparticles by Atomic Layer Deposition: Comparison with Organic Spacing Layers. *Appl. Phys. Lett.* **2014**, *104*, 023109.
(28) Mock, J. J.; Hill, R. T.; Degiron, A.; Zauscher, S.; Chilkoti, A.; Smith, D. R. Distance-Dependent Plasmon Resonant Coupling between a Gold Nanoparticle and Gold Film. *Nano Lett.* **2008**, *8*, 2245−2252.
(29) Lei, D. Y.; Fernandez-Dominguez, A. I.; Sonnefraud, Y.; Appavoo, K.; Haglund, R. F.; Pendry, J. B.; Maier, S. A. Revealing Plasmonic Gap Modes in Particle-on-Film Systems Using Dark-Field Spectroscopy. *ACS Nano* **2012**, *6*, 1380−1386.
(30) Landau, L. On the Vibration of the Electronic Plasma. *J. Phys. USSR* **1946**, *10*, 25−34.
(31) Apell, P.; Monreal, R.; Lundqvist, S. Photoluminescence of Noble-Metals. *Phys. Scr.* **1988**, *38*, 174−179.
(32) Romaniello, P.; de Boeij, P. L. The Role of Relativity in the Optical Response of Gold within the Time-Dependent Current-Density-Functional Theory. *J. Chem. Phys.* **2005**, *122*, 164303.
(33) *CST Microwave Studio*; Computer Simulation Technology: Darmstadt, Germany, 2013.
(34) Johnson, P. B.; Christy, R. W. Optical Constants of the Noble Metals. *Phys. Rev. B* **1972**, *6*, 4370−4379.
(35) Lichtenstein, T. *Handbook of Thin Film Materials*; University of Rochester: Rochester, New York, 1979.
(36) Jackson, J. D. *Classical Electrodynamics*; Wiley: New York, 1962.